

Solar radiative biases in deep convective regimes: Possible implications for dynamical feedback

By A. M. TOMPKINS^{1*} and F. DI GIUSEPPE²

¹*European Centre for Medium-Range Weather Forecasts, UK*

²*Environmental Systems Science Centre, University of Reading, UK*

(Received 24 April 2002; revised 7 November 2002)

SUMMARY

There is increasing evidence that interactions between radiation and convectively determined water vapour and cloud fields can have a significant dynamical impact on the tropical circulation. However, the use of a one-dimensional (1D) independent column method for the calculation of solar fluxes in cloud-resolving or mesoscale models could possibly misrepresent this feedback. This is investigated by calculating 1D and full three-dimensional (3D) solar fluxes through a 3D field of deep convective clouds generated using a high-resolution cloud-resolving model, and diagnosing the clear-sky subsidence velocities required to balance this if a state of radiative convective equilibrium were to exist. The mean clear-sky solar radiative heating rate is found to change by up to 15%. At low sun angles the shading of the clear-sky regions implies a reduction of net clear-sky heating rates. In contrast, at higher solar elevations the scattering effect dominates shading and the clear-sky heating rates are enhanced, implying an enhancement of the diurnal cycle. However, since the 1D/3D heating-rate differences in the clear sky increase smoothly from zero at the tropopause to their maximum value near the surface, the vertical gradient and thus the impact on the vertical profile of entrainment and detrainment into the convective regions is negligibly small. This implies that the strong radiative dynamical feedbacks so far documented in cloud-ensemble models cannot be discounted on the grounds of their use of an independent column calculation for the solar radiative transfer. That said, the substantial bias noted in surface downward solar fluxes could result in a substantial impact in convective organization if an interactive land surface were used as a lower boundary condition.

KEYWORDS: Plane parallel error

1. INTRODUCTION

Global model studies have shown that the interaction between radiation and clouds can have an important impact on the simulated tropical circulation (e.g. Slingo and Slingo 1988; Randall *et al.* 1989; Sherwood *et al.* 1994; Lohmann and Roeckner 1995; Lee *et al.* 2001). Recently, attention has focused on identifying the mechanisms and spatial scales that define the dynamical feedback between convective clouds, the associated water-vapour field and radiation. Raymond (2000) suggested that the interaction between thermal radiation and clouds could enhance the Hadley circulation, and both Nilsson and Emanuel (1999) and Raymond and Zeng (2000) found radiative–dynamical instabilities in idealized two-column models of the tropics. The above studies have a feature in common, in that they were forced to represent the effect of convection by parametrization schemes of varying complexity. Determining the radiative dynamical feedback in observations is difficult, although attempts have been made by Sohn (1999) and Bergman and Hendon (2000).

An alternative approach is to use higher-resolution models that resolve convective motion, therefore absolving the requirement for a parametrization scheme. To date, computational expense has restricted their use (in three dimensions) to mesoscale domains of $O(100\text{ km})$, but even at these scales Tompkins and Craig (1998a) found that strong mesoscale organization of deep convection occurred in a cloud-resolving model (CRM) using an interactive radiation scheme for both the short-wave and infrared spectra. When the interactive radiative forcing was replaced by a simple spatially and temporally homogeneous cooling of the same magnitude, the organization was quickly destroyed, with the convective events becoming randomly distributed, proving that radiative feedbacks with convection were the main cause of the organization. Grabowski and Moncrieff (2002) also found that interactions with radiation have a large impact on convective organization in a large-domain two-dimensional (2D) CRM, with the creation of strong mesoscale organization when radiation was allowed to respond to the water vapour and cloud structures.

The current practice for implementing radiative schemes in CRMs is to make an independent calculation for each model column (referred to as the independent column approximation (ICA)), due to the

* Corresponding author: ECMWF, Shinfield Park, Reading RG2 9AX, UK. e-mail: Tompkins@ecmwf.int
© Royal Meteorological Society, 2003.

prohibitive computational expense of a full three-dimensional (3D) radiative calculation. With horizontal resolutions finer than 2 km, one issue is whether the interaction with solar radiation is adequately represented with an ICA calculation, especially for low solar angles. This note attempts to address this question by comparing a full 3D and ICA solar radiative-transfer calculation for a 3D scene of deep convective clouds generated by a CRM.

Some previous investigations using model-generated deep convective fields have been conducted in two dimensions (Fu *et al.* 2000), but Tompkins (2000) argued strongly that 2D geometry artificially widens the scale of convective organization, which could cause 3D radiative effects to be underestimated. A detailed investigation of 3D effects associated with 400 km² 3D cloud fields in situations of scattered and organized convection generated by a CRM of 2 km horizontal resolution was conducted by Barker *et al.* (1999). They found that in the case of scattered convection the differences between 3D Monte Carlo and ICA calculations were small. However, a notable feature of the microphysical scheme used in the CRM of that study is that all the situations were virtually overcast (Grabowski *et al.* 1998). Differences between ICA and full 3D radiative calculations are expected to be minimized as cloud cover approaches unity. Barker *et al.* (1999) also examined the bias neglecting all ice cloud. Again the ICA bias was small, as expected considering the consequential lack of high-level anvil cloud, with low-level warm-rain part of deep convective cores likely to be arranged in a maximally overlapped geometry. Similarly, Barker *et al.* (1998) examined a 3D field with high-cloud coverage around 6 km. The isolated convective turrets that penetrated through to the tropopause had little effect on the ICA bias due to the presence of this underlying cloud shield.

The aim of this note is, therefore, to examine the difference in ICA and 3D radiative heating rates using a scene taken from the CRM simulations of Tompkins (2001), which simulated tropical radiative convective equilibrium in a zero wind-shear situation. The domain of this simulation was 90 by 90 km in the horizontal, smaller than that of Barker *et al.* (1999), but with a much higher horizontal resolution of 350 m in order to resolve the structure of the convective towers in addition to the anvil-cloud shield. The cloud cover has a similar form to the ‘scattered convection’ case of Barker *et al.* (1999), with peaks at the deep convective detrainment level in the upper troposphere and in the shallow convective layer. However, due to the differences in the model microphysics the anvil extent is much less, with individual anvils typically extending to a radius of 15 to 25 km, typical for this situation in low wind-shear conditions. Due to the computational demands of calculating 3D radiative transfer through such a field, only one scene is examined. However, since the domain was large enough to always contain an ensemble of active convective events, the characteristics of the scene examined are representative for the entire simulation. The reader is referred to Tompkins (2001) for details of the CRM simulation and set-up. These biases are then considered in the context of mesoscale dynamics, and the possible implications for the organization of convection simulated by CRMs are discussed.

2. METHODOLOGY

On a tropics-wide scale, clear-sky subsidence warming balances radiative cooling in a quasi-equilibrium state where longer-term temperature tendencies are small. This must also be approximately valid over smaller scales for the clear-sky areas between deep convective clouds in regions of mean ascent (cf. Emanuel *et al.* 1994). This relation is thus used to assess crudely the magnitude of the dynamical response to 3D radiative effects. Radiative heating is converted using the temperature lapse rate to subsidence velocity:

$$w = \frac{Q_{\theta}}{d\theta/dz}, \quad (1)$$

where Q_{θ} is the mean net radiative (potential temperature, θ) heating rate in clear-sky regions. A column is defined as clear sky provided that no grid point in the vertical has a cloud condensate mixing ratio exceeding the threshold of 5×10^{-6} kg kg⁻¹. We can then examine the mass convergence/divergence implied by quasi-equilibrium by vertical differentiation of the subsidence profiles. Mapes (2001) uses this relationship for an idealized case. This diagnostic relationship simply gives an ‘initial response’ view of the dynamical interaction. In reality, convective mass fluxes would not exactly counteract radiative cooling, and the imbalance would produce net temperature (and moisture) tendencies, with the system moving towards a new equilibrium state. However, we maintain that these derived velocity profiles still provide useful information, particularly while integrations of CRMs coupled to full 3D radiative codes remain prohibitively expensive, since they give an estimate of the sign and magnitude of expected response, assuming that the system is not overly nonlinear and is not perturbed into a completely new equilibrium regime, if such multiple equilibria can exist (Rennó 1997).

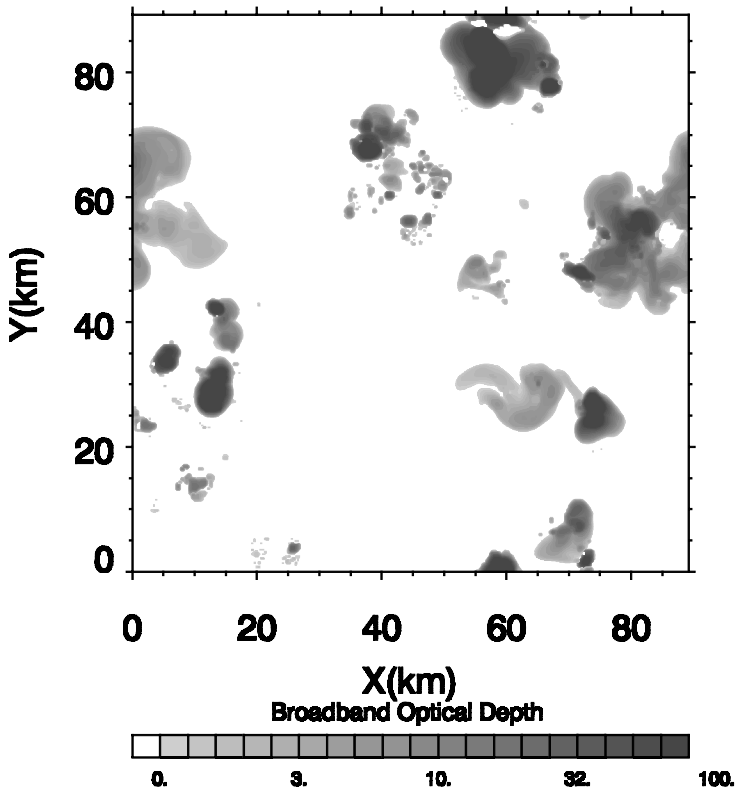


Figure 1. Broadband optical depth for the convective cloud field used in this study. See text for details of the calculation.

3. RADIATIVE CALCULATION

The solar radiative-transfer calculations were performed using SHDOM, a spherical harmonics code, which is described in detail by Evans (1998). Along each angular direction, the cloud liquid- (or ice-) water content is obtained by interpolation between grid points. Where strong gradients exist, for instance at cloud boundaries, cells are divided into a number of subgrid cells to avoid inaccuracy. This study adopts a medium angular resolution of 8 azimuth and 16 zenith angles, while a sensitive cell-splitting threshold is used that only allows a 10% variation in cloud properties between cells in order to handle the highly variable source function that exists in this type of cloud field. Using higher-resolution tests on smaller domains, the numerical accuracy was assessed at approximately 1% of the integrated up-welling and down-welling fluxes.

In this initial investigation, only the cloud mass varies in the horizontal; water vapour and temperature are functions of height only. The role of lateral humidity variations will be the subject of future investigation. Water and ice phases are considered, and in both cases Mie theory is used to derive the extinction coefficients. The size particle distribution is modelled using a gamma function with effective radius ranging between 0.5 and 25 microns (mode of 10 microns) for the water droplets and 10 and 50 microns (mode of 30 microns) for the ice crystals, being in both cases constrained by the constant particle concentration numbers of 50 and 30 cm^{-3} , respectively. The CRM integration was conducted over an ocean surface and for simplicity the surface albedo is thus set to zero.

A spectral band calculation is performed using the k-distribution model of Fu and Liou (1992). Six bands cover the solar spectrum between 0.2 and 4 microns. Rayleigh scattering extinction is included. Above the CRM domain seven additional atmospheric levels are placed between 20 km and 100 km which are interpolated using tropical standard profiles (McClatchey *et al.* 1972).

For illustrative purposes, the broadband optical thickness (τ_b) is shown for the CRM scene considered (Fig. 1), which is calculated as a weighted mean of the optical thickness in each of the six short-wave

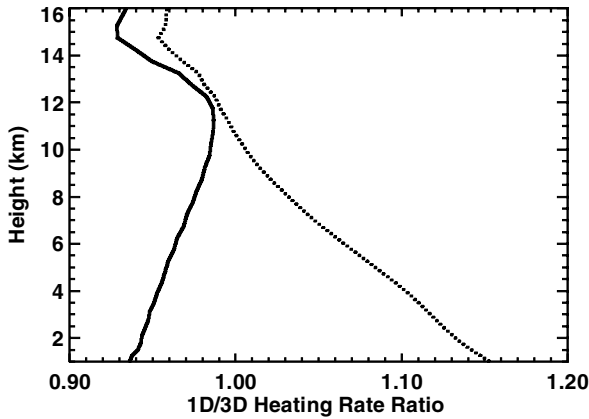


Figure 2. Ratio of 1D to 3D solar heating rates for sun over head (full line) and 60° solar zenith angle (dotted line) cases.

spectral bands according to

$$\tau_b = \log\left(\frac{\sum S_i e^{-\tau_i}}{\sum S_i}\right) \quad (2)$$

where S_i is the flux of band i . The mean optical thickness is estimated at 70 with a maximum in the domain of 200. The narrow but optically opaque updraught cores are apparent in addition to the optically thinner cirrus anvil outflow regions, which can exceed 30 km in horizontal extent.

Using this cloud field, two experiments have been performed for solar zenith angles (SZAs) of 0 (sun overhead) and 60° . The infrared (IR) clear-sky calculation is performed using Mlawer *et al.* (1997).

4. RESULTS

(a) Clear-sky biases

Figure 2 shows the relative change in clear-sky heating rates when horizontal radiative flux transfer is taken into account, for both SZAs. The more substantial differences between the 3D and one-dimensional (1D) calculations are notable below about 8 km in altitude, below the level of deep convective detrainment. Clearly 3D radiative transfer has a non-negligible effect, particularly at lower levels, where differences of up to 15% are noted, which is equivalent to a heating-rate difference of approximately 0.4 K day^{-1} . These differences substantially exceed those previously reported by Barker *et al.* (1999) and Fu *et al.* (2000) for deep convective cases. This presumably as a result of the different cloud geometry and lower cloud cover in the situation investigated here, in addition to the higher resolution used in this study. It should also be noted that the domain mean biases given by Barker *et al.* (1999) and Fu *et al.* (2000) will also be reduced by cancellation between cloudy and clear regions, which is not the case if only clear-sky columns are examined. Interestingly, at the low SZA of 60° , the ICA gives larger heating rates than the associated 3D calculation, while with the sun overhead the opposite is true. This change in sign was also observed previously in the investigations of O'Hirok and Gautier (1998), Barker *et al.* (1998) and Fu *et al.* (2000).

The reversal of this effect points to the increased role that shading takes in cloud systems that have aspect ratios approaching unity. In contrast to horizontally extended clouds, these tall and optically thick deep convective systems produce extensive shading at low sun angles, which is not compensated for by increased flux convergence on the sunny side of the cloud. This is observed in Fig. 3, which shows vertical and horizontal mean 1D/3D heating-rate differences through the domain, and clearly indicates the strong shading of the anvil and convective core downstream. The convective cores are easy to locate since they are opaque to solar radiative transfer, while some of the anvil regions are transparent enough to permit significant solar transfer. Although the mean clear-sky heating-rate difference is limited to 15%, point heating rates can differ by up to 1.5 K day^{-1} . The low-sun-angle results contrast with the behaviour for the sun overhead in which the shading of clear-sky columns is obviously eliminated (not shown). It is apparent that the geometry and organization of the deep convection systems in a 3D CRM, where inter-cloud distances are of a similar order of magnitude to the height of the cloud systems, will produce much

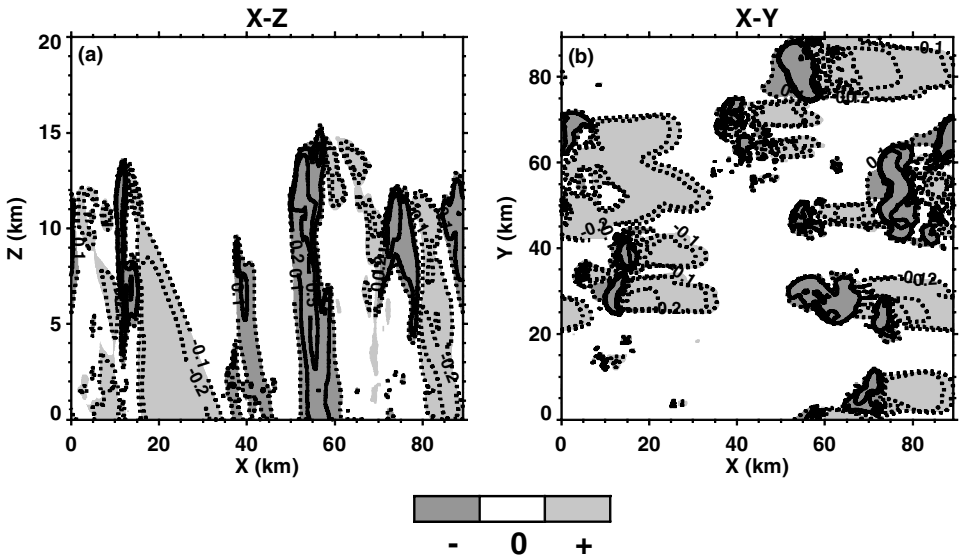


Figure 3. (a) Vertical and (b) horizontal mean difference between 1D and 3D heating rates for a solar zenith angle of 60° . The contour interval is 0.1, 0.2 and 0.5 K day^{-1} , with negative values shown dotted. The shaded regions indicate regions where the absolute difference exceeds 0.05 K day^{-1} .

larger estimations of the 3D/ICA radiative differences than a 2D CRM, since the latter artificially widens the inter-cloud (or cloud cluster) spacing, as demonstrated by Tompkins (2000).

To examine the scale dependency of the biases, Fig. 4 shows the root-mean-square (RMS) error of the clear-sky solar heating-rate bias as a function of scale, by dividing the domain into progressively smaller regions and taking the average of the clear-sky bias in each sub-region. The result is shown only for the 60° SZA case where mean biases are more significant, and reveals a sharp increase in the heating-rate bias as the horizontal scale becomes comparable with the typical anvil size, again highlighting the importance of the cloud geometry in determining bias magnitude. Shallow convective systems with a similar cloud coverage but lacking anvil structure are likely to have more limited ICA biases.

(b) Dynamical implications

More detailed investigation of the radiative effects of the 3D calculation will be performed in a companion paper. Here the desire is to estimate how these clear-sky changes would affect the clear-sky subsidence profiles, indicating an approximate dynamical response. The derived clear-sky subsidence velocity is shown in Fig. 5 which uses the European Centre for Medium-Range Weather Forecasts IR calculation for the clear-sky points, and the domain mean potential-temperature lapse rate from the CRM, as outlined above. The diagram indicates that in the 60° SZA case, the shading reduces the subsidence rate throughout the troposphere, as expected. The smaller lapse rate in the upper troposphere does not compensate for the reduction in radiative heating differences there, and the subsidence rates are essentially identical above 8–9 km.

Note that the subsidence rates show significant noise. This is caused by heating-rate and lapse-rate changes corresponding to vertical moist structures. The smooth moisture structure shown in the tephigram of Tompkins and Craig (1998a) is only valid in a time-mean sense. At any instant, the CRM shows significant vertical structure in the moisture profiles, where moist layers resulting from earlier convective detrainment are separated by much drier layers; the consequence of relative convective inactivity. These structures are common in the tropics, with advection playing a greater role (e.g. Yoneyama and Parsons 1999), and Mapes and Zuidema (1996) discuss the radiative and dynamical properties of such ‘dry tongues’. The consequence is that the smooth subsidence and related convergence/divergence profiles, derived by Mapes (2001) for an idealized situation, are not obtainable for the general-circulation modeled grid box used here at one particular instant. Since convection organizes on scales far exceeding this domain of 100 km, it is likely that averages over the radiative subsidence time-scale of around 30 days (Emanuel *et al.* 1994; Tompkins and Craig 1998b), or over greater spatial scales, would be necessary to derive such profiles.

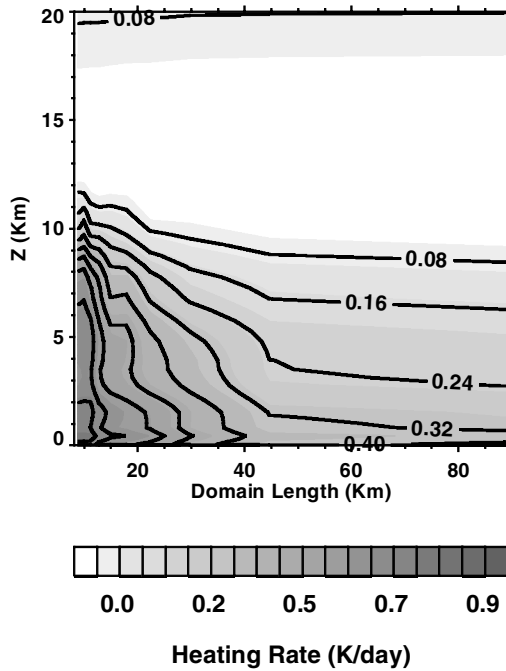


Figure 4. Root-mean-square error in clear-sky solar heating rates for a solar zenith angle of 60° as a function of horizontal averaging scale.

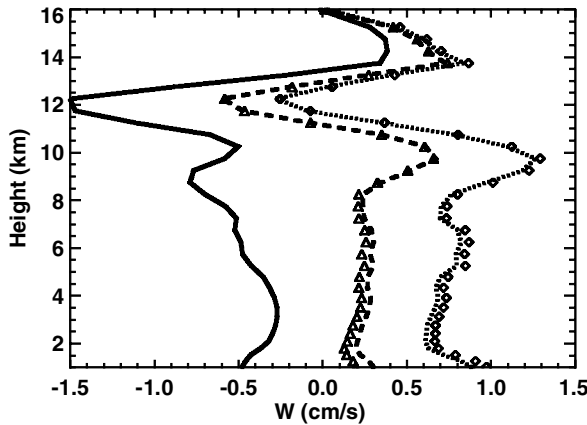


Figure 5. Equivalent clear-sky subsidence velocity required to balance the 1D radiative heating in equilibrium for night (full line), solar zenith angle (SZA) = 60° (dashed line) and sun overhead (dotted line). The triangles and diamond symbols represent the equivalent 3D subsidence velocities for the SZA = 60° and sun overhead cases, respectively.

Although the solar radiative-heating rates change by up to 15%, this is equivalent to a smaller relative change in the clear-sky subsidence velocities when considered in the context of the diurnal cycle. For the 60° SZA case, in the mean over the layer between the surface and 8 km, the 3D radiative transfer reduces the offset of solar radiation, while in the case of the sun overhead, the opposite is true. It is therefore apparent that 3D radiative transfer has the effect of sharpening the diurnal cycle in the seasonal conditions where the sun is able to attain low SZAs, since the range of the dynamical response between night and day is increased in these cases.

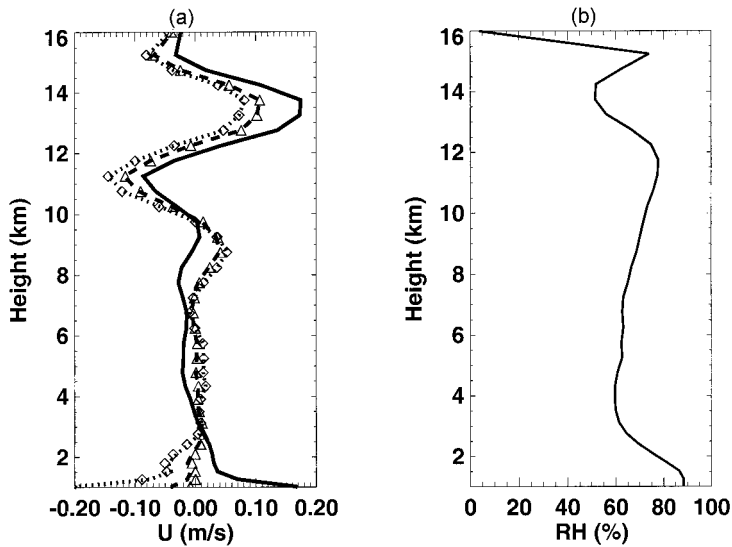


Figure 6. Comparison of (a) horizontal convergent/divergent wind for the clear-sky region for night (full line), solar zenith angle (SZA) = 60° (dashed line) and sun overhead (dotted line) and (b) relative humidity. Positive winds implies detrainment from convective areas into the clear-sky regions. The triangles and diamond symbols represent the equivalent 3D subsidence velocities for the SZA = 60° and sun overhead cases, respectively.

The net horizontal velocity into/out of the clear-sky region can be calculated by mass conservation and assuming a cylindrical clear-sky geometry: $U = \frac{1}{2} \sqrt{(1-C)/\pi} dw/dz$ (where C is the cloud-covered area), and is compared with the relative humidity (RH) in Fig. 6. A divergence/convergence dipole structure exists in the upper troposphere of strong detrainment into the clear-sky region between 12 and 14 km residing over an entrainment layer. This structure results from the IR cooling profile, which in turn is responding to the RH structure of the atmosphere. This feature, while disjunct from the solar-transfer dimensionality theme, merits a minor digression. It is intriguing that the detrainment layer occurs precisely at the levels where RH is at a minimum while the entrainment region below 12 km altitude coincides with a RH maximum (actually resulting from a strong *detrainment* in the original CRM simulation). The reason for this is clear since the top of a moist layer will be subject to strong cooling due to the dry layer above (see schematic of Mapes and Zuidema (1996)), increasing the subsidence velocity, and enhancing detrainment at and above the moist-dry interface. This enhancement of detrainment into dry layers presumably leads to a wider spectra of cloud-top heights when convection is permitted to interact with radiation, resulting in a well mixed upper troposphere and smaller humidity gradients. Mapes and Zuidema (1996) also discuss that strong vertical humidity gradients additionally permit the development of limited-magnitude stable layers at the interface, since gravity waves propagate these high vertical wave number, mesoscale virtual-temperature structures away less efficiently.

Below this level there is little detrainment/entrainment throughout the troposphere, with most of the divergence/convergence occurring below 2 km, although the profiles there are not reliable since diffusive heat transport is neglected in this simplistic calculation of subsidence velocities. Finally, no discernible difference is seen when comparing the 1D and 3D entrainment/detrainment rates. This is because, although significant differences between heating rates occur, in the clear sky the differences increase gradually from the detrainment level downwards, in contrast to the in-cloud solar-heating rates which have large vertical gradients in heating-rate differences (not shown). Thus, since it is the vertical gradient of the solar heating-rate differences that is important for entrainment/detrainment profiles, it is apparent that using an ICA method of calculation for the solar radiative transfer in CRM simulations will not affect the assessment of mesoscale radiative/convective dynamical feedback. That said, it is possible that larger differences could be found if the convection was occurring over a higher albedo land surface.

(c) Surface interaction

The above discussion concentrated on the dynamical impact of atmospheric heating-rate biases. This is relevant for many previous CRM investigations conducted over sea surfaces, usually with fixed imposed

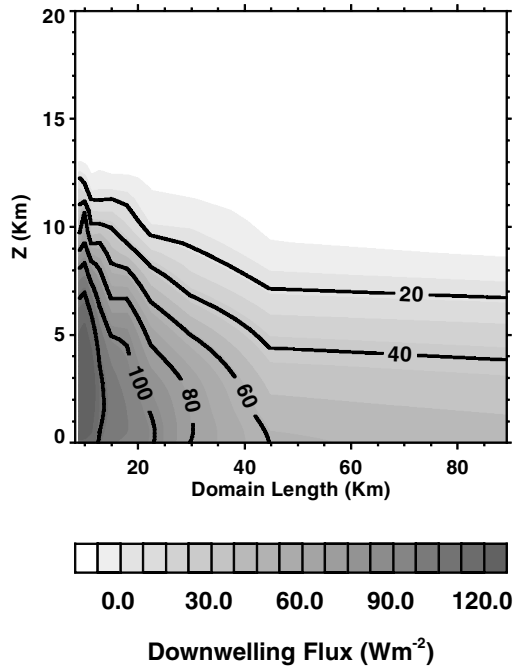


Figure 7. Root-mean-square error in clear-sky down-welling solar fluxes for a solar zenith angle of 60° as a function of horizontal averaging scale.

characteristics. However, over land surfaces it is possible that significant organizational feedback could occur due to biases in down-welling solar fluxes, which could be relevant since CRMs are now being coupled to more complex interactive surface schemes (e.g. Costa *et al.* 2001). Thus, Fig. 7 shows the RMS error in the clear-sky down-welling solar flux as a function of scale for the 60° SZA. The ICA bias has a similar form to the heating-rate bias, increasing sharply for scales less than 30 km, for which the bias exceeds 100 W m^{-2} . The magnitude of this indicates that over interactive land surfaces the organization of convection could possibly undergo strong modification if a fully interactive 3D assessment of solar radiative transfer were used rather than the current ICA implementation.

5. SUMMARY

In summary, it is seen that for unorganized deep convective regimes with anvil-cloud fractions that are significantly smaller than unity, as investigated here, the radiative effect of allowing 3D horizontal transfer can change the clear-sky solar-heating rates by as much as 15%. The net effect of the horizontal flux transfer was to increase clear-sky heating rates when the sun is overhead due to flux divergence from the cloud regions, while at low sun angles the shading effect of the cumulus towers and associated anvil regions dominates, reducing the clear-sky heating rates, producing a sharpening of the clear-sky diurnal cycle. The impact on the convergence/divergence into the clear-sky region over the mesoscale is negligible, since the vertical gradient of the 1D/3D clear-sky heating-rate differences in the clear sky is small. This implies that the existence of strong dynamical feedbacks between convection and radiation documented in the CRM studies of Tompkins and Craig (1998a) and Grabowski and Moncrieff (2002) can be assumed not to be an artifact of the radiation calculation method that assesses solar heating rates independently column by column, neglecting 3D transfer. It remains to be established what determines the scale selection of such a dynamical interaction. Finally, the significant RMS errors in surface down-welling solar fluxes which can exceed 100 W m^{-2} could imply a strong dynamical feedback if an interactive land surface were used as a lower boundary condition.

ACKNOWLEDGEMENTS

The radiation calculation was performed at Manchester Supercomputer facilities with the use of the UK Universities' Global Atmospheric Modelling Programme resources, and Lois Steenman-Clark is thanked for arranging this provision. The authors express their gratitude to Frank Evans for providing his radiation code and advice on its use. The Met Office made available the cloud-resolving model. Kevin Hodges is also thanked for his aid.

REFERENCES

- Barker, H. W., Morcrette, J. J. and Alexander, G. D. 1998 Broadband solar fluxes and heating rates for atmospheres with 3D broken clouds. *Q. J. R. Meteorol. Soc.*, **124**, 1245–1271
- Barker, H. W., Stephens, G. L. and Fu, Q. 1999 The sensitivity of domain-averaged solar fluxes to assumptions about cloud geometry. *Q. J. R. Meteorol. Soc.*, **125**, 2127–2152
- Bergman, J. W. and Hendon, H. H. 2000 Cloud radiative forcing of the low-latitude tropospheric circulation: Linear calculations. *J. Atmos. Sci.*, **57**, 2225–2245
- Costa, A. A., Cotton, W. R., Walko, R. L. and Pielke, R. A. 2001 Coupled ocean–cloud-resolving simulations of the air–sea interaction over the equatorial western Pacific. *J. Atmos. Sci.*, **58**, 3357–3375
- Emanuel, K. A., Neelin, J. D. and Bretherton, C. S. 1994 On large-scale circulations in convecting atmospheres. *Q. J. R. Meteorol. Soc.*, **120**, 1111–1143
- Evans, K. F. 1998 The spherical harmonics discrete ordinate method for three-dimensional atmospheric radiative transfer. *J. Atmos. Sci.*, **55**, 429–446
- Fu, Q. and Liou, K. N. 1992 On the correlated k-distribution method for radiative-transfer in nonhomogeneous atmospheres. *J. Atmos. Sci.*, **49**, 2139–2156
- Fu, Q., Cribb, M. C., Barker, H. W., Krueger, S. K. and Grossman, A. 2000 Cloud geometry effects on atmospheric solar absorption. *J. Atmos. Sci.*, **57**, 1156–1168
- Grabowski, W. W. and Moncrieff, M. W. 2002 Large-scale organization of tropical convection in two-dimensional explicit numerical simulations: Effects of interactive radiation. *Q. J. R. Meteorol. Soc.*, **128**, 2349–2375
- Grabowski, W. W., Wu, X., Moncrieff, M. W. and Hall, W. D. 1998 Cloud-resolving modeling of cloud systems during phase III of GATE. Part II: Effects of resolution and the third spatial dimension. *J. Atmos. Sci.*, **55**, 3264–3282
- Lee, M. I., Kang, I. S., Kim, J. K. and Mapes, B. E. 2001 Influence of cloud–radiation interaction on simulating tropical intraseasonal oscillation with an atmospheric general circulation model. *J. Geophys. Res.*, **106**, 14219–14233
- Lohmann, U. and Roeckner, E. 1995 Influence of cirrus cloud radiative forcing on climate and climate sensitivity in a general-circulation model. *J. Geophys. Res.*, **100**, 16305–16323
- McClatchey, R. A., Fenn, R. W., Selby, J. E. A., Volz, F. E. and Garing, J. S. 1972 'Optical properties of the atmosphere'. Technical Report AFCRL-72-0497, Hanscom Air Force Base, Bedford, MA, USA
- Mapes, B. E. 2001 Water's two height scales: The moist adiabat and the radiative troposphere. *Q. J. R. Meteorol. Soc.*, **127**, 2353–2366
- Mapes, B. E. and Zuidema, P. 1996 Radiative–dynamical consequences of dry tongues in the tropical troposphere. *J. Atmos. Sci.*, **53**, 620–638
- Mlawer, E. J., Taubman, S. J., Brown, P. D., Iacono, M. J. and Clough, S. A. 1997 Radiative transfer for inhomogeneous atmospheres: RRTM, a validated correlated-k model for the long wave. *J. Geophys. Res.*, **102**, 16663–16682
- Nilsson, J. and Emanuel, K. A. 1999 Equilibrium atmospheres of a two-column radiative–convective model. *Q. J. R. Meteorol. Soc.*, **125**, 2239–2264
- O'Hirok, W. and Gautier, C. 1998 A three-dimensional radiative transfer model to investigate the solar radiation within a cloudy atmosphere. Part I: Spatial effects. *J. Atmos. Sci.*, **55**, 2162–2179
- Randall, D. A., Harshvardhan, Dazlich, D. A. and Corsetti, T. G. 1989 Interactions among radiation, convection, and large-scale dynamics in a general-circulation model. *J. Atmos. Sci.*, **46**, 1943–1970
- Raymond, D. J. 2000 The Hadley circulation as a radiative–convective instability. *J. Atmos. Sci.*, **57**, 1286–1297
- Raymond, D. J. and Zeng, X. 2000 Instability and large-scale circulations in a two-column model of the tropical troposphere. *Q. J. R. Meteorol. Soc.*, **126**, 3117–3135

- Rennó, N. O. 1997 Multiple equilibria in radiative–convective atmospheres. *Tellus*, **49**, 423–438
- Sherwood, S. C., Ramanathan, V., Barnett, T. P., Tyree, M. K. and Roeckner, E. 1994 Response of an atmospheric general-circulation model to radiative forcing of tropical clouds. *J. Geophys. Res.*, **99**, 20829–20845
- Slingo, A. and Slingo, J. M. 1988 The response of a general-circulation model to cloud long-wave radiative forcing. 1. Introduction and initial experiments. *Q. J. R. Meteorol. Soc.*, **114**, 1027–1062
- Sohn, B. J. 1999 Cloud-induced infrared radiative heating and its implications for large-scale tropical circulations. *J. Atmos. Sci.*, **56**, 2657–2672
- Tompkins, A. M. 2000 The impact of dimensionality on long-term cloud resolving model simulations. *Mon. Weather Rev.*, **128**, 1521–1535
- 2001 Organization of tropical convection in low vertical wind shears: The role of cold pools. *J. Atmos. Sci.*, **58**, 1650–1672
- Tompkins, A. M. and Craig, G. C. 1998a Radiative–convective equilibrium in a three-dimensional cloud ensemble model. *Q. J. R. Meteorol. Soc.*, **124**, 2073–2097
- 1998b Time-scales of adjustment to radiative–convective equilibrium in the tropical atmosphere. *Q. J. R. Meteorol. Soc.*, **124**, 2693–2713
- Yoneyama, K. and Parsons, D. B. 1999 A proposed mechanism for the intrusion of dry air into the tropical western Pacific region. *J. Atmos. Sci.*, **56**, 1524–1546